Discrete element method analysis of single wheel performance for a small lunar rover on sloped terrain

AUTHOR(S):

Nakashima, H.; Fujii, H.; Oida, A.; Momozu, M.; Kanamori, H.; Aoki, S.; Yokoyama, T.; Shimizu, H.; Miyasaka, J.; Ohdoi, K.

CITATION:

Nakashima, H. ...[et al]. Discrete element method analysis of single wheel performance for a small lunar rover on sloped terrain. Journal of Terramechanics 2010, 47(5): 307-321

ISSUE DATE:

2010-10

URL:

http://hdl.handle.net/2433/126852

Discrete element method analysis of single wheel performance for a small lunar rover on sloped terrain

H. Nakashima [a,*], H. Fujii [b], A. Oida [a], M. Momozu [c], H. Kanamori [d], S. Aoki [d], T. Yokoyama [e], H. Shimizu [a], J. Miyasaka [a], K. Ohdoi [a]

[a] *Division of Environmental Science & Technology, Graduate School of Agriculture, Kyoto University, Kyoto 606-8502, JAPAN*

[b] *Toyota Motor Corporation, Toyota, Aichi 471-8571, JAPAN*

[c] *Bridgestone Corporation, Kodaira, Tokyo 187-8531, JAPAN*

[d] *Institute of Technology, Shimizu Corporation, Koto-ku, Tokyo 135-8530, JAPAN*

[e] *College of Science & Engineering, Ritsumeikan University, Kusatsu, Shiga 525-8577, JAPAN*

Abstract

The purpose of this study is to analyze the performance of a lugged wheel for a lunar micro rover on sloped terrain by a 2D discrete element method (DEM), which was initially developed for horizontal terrain. To confirm the applicability of DEM for sloped terrain locomotion, the relationships of slope angle with slip, wheel sinkage and wheel torque obtained by DEM, were compared with experimental results measured using a slope test bed consisting of a soil bin filled with lunar regolith simulant. Among the lug parameters investigated, a lugged wheel with rim diameter of 250 mm, width of 100 mm, lug height of 10 mm, lug thickness of 5 mm, and total lug number of 18 was found, on average, to perform excellently in terms of metrics, such as slope angle for 20% slip, power number for self-propelled point, power number for 15-degree-slope and power number for 20% slip. The estimation of wheel performance over sloped lunar terrain showed an increase in wheel slip, and the possibility exists that the selected lugged wheel will not be able to move up a slope steeper than 20 degrees.

Key words: Computational mechanics; Discrete element method; Soil-wheel system; Slope; Wheel performance; Lug; Lunar rover

* Corresponding author. Tel.: +81-75-753-6164; Fax.: +81-75-753-6165.
Email address: hiron@kais.kyoto-u.ac.jp (H. Nakashima).

Nomenclature

μ friction coefficient between soil elements
μ^L friction coefficient between soil element and wheel (or lug) element
μ^w friction coefficient between soil element and wall element
ω angular velocity of wheel
ϕ angle of internal friction
ρ density of soil element
ρ_d dry bulk density
ρ_e representative bulk density for damping coefficient calculation in DEM
ρ_{max} maximum dry bulk density
ρ_{min} minimum dry bulk density
θ inclination angle of slope
$\theta_{20\%}$ inclination angle of slope at 20% slip
A_l total section area of lugs, such that $L_n B L_T$
A_w area of possible contacting surface of wheel rim, such that $\pi B D_0$
B width of wheel
c cohesion
C_l percent cover of total section area of lugs over area of wheel surface without lugs, such that $C_l = A_l/A_w$
C_n normal damping coefficient in DEM
C_t tangential damping coefficient in DEM
D outermost diameter of a wheel inclusive of lug height
D_0 rim diameter of a wheel
D_r relative density of lunar regolith simulant
f_x^+ positive x-component of contact reaction w. r. t. local axis
f_x^- negative x-component of contact reaction w. r. t. local axis
H gross traction in slope locomotion, obtained as $H = \sum f_x^+$
i slip of a wheel in slope locomotion, such that $i = 1 - (V_s/r_w\omega)$
K_n normal spring constant between soil elements
K_n^L normal spring constant between soil element and wheel (or lug) element
K_n^w normal spring constant between soil element and wall element
K_t tangential spring constant between soil elements
K_t^L tangential spring constant between soil element and wheel (or lug) element
K_t^w tangential spring constant between soil element and wall element
L_H height of lug
L_n total number of lug for a wheel
L_T lug thickness
m_e equivalent mass of soil element, defined as $\rho_e\times$ (volume of largest soil element)
P drawbar pull
P_d net traction in slope locomotion, obtained as $P_d = H - R_r$
PN power number, defined by $T\omega/WV_a$
P/W pull coefficient, dimensionless, with respect to drawbar pull P or P_x

P_x drawbar pull w.r.t. local x-axis, $P_x = W \sin\theta$
R_r motion resistance in slope locomotion, obtained as $R_r = \sum f_x^-$
r_w rolling radius of a wheel, approximated to be an outermost radius of wheel as $r_w = D/2$
T wheel torque, obtained as $T = Hr_w$
$T/(Wr_w)$ torque coefficient
V_s translational velocity of wheel along local x-axis
V_X translational velocity of wheel along global X-axis
V_Y translational velocity of wheel along global Y-axis
W Vertical contact load of wheel w. r. t. global axis
W_y normal contact load of wheel w. r. t. local axis, $W_y = W \cos\theta$
x abscissa of local coordinate system on a slope, positive for ascending direction
X abscissa of global coordinate system, positive for rightward direction
y ordinate of local coordinate system on a slope
Y ordinate of global coordinate system, positive for upward direction
z sinkage of wheel w. r. t. local y-axis
Z sinkage of wheel w. r. t. global Y-axis
z_a average sinkage of wheel w. r. t. local y-axis
Z_e depth of soil w. r. t. global Y-axis

1 Introduction

The Selenological and Engineering Explorer (SELENE) was a Japanese lunar exploration project that ran from December 2007 to June 2009. Using a remote sensing system on an observational orbiter, named “Kaguya,” SELENE obtained the first precise data on lunar surface geometry and mineral composition. A follow-up project, SELENE-2, is now under discussion at JAXA. Its main mission objectives would be to land on the Moon and obtain in situ geological samples using a small robotic rover [1]. To keep the payload of the H-II rocket to a minimum, the rover vehicle must be as small and light as possible. The envisaged maximum mass of the rover is 100 kg [2]. The rover can use either wheels or tracks for locomotion.

Since one of the candidate landing sites for SELENE-2 would be around the central peak of a crater, which should provide abundant geological information on the origin of the Moon, initial discussions on terramechanics for SELENE-2 had been focused on the mobility of a rover over the soft powdery lunar regolith accumulated over the peak. For this reason, an experimental investigation was started in an indoor horizontal soil bin with a lunar regolith simulant at Tsukuba Space Center (TSC) of NASDA (currently JAXA). Experiments with a rigid wheel resembling a conventional tire with no lugs, showed difficulty of locomotion even on horizontal terrain condition for a smaller drawbar load [3]. Moreover, developing a performance prediction model for such a 3D wheel shape proved difficult. Therefore, we

decided to develop simpler wheels with straight lugs, which may be approximated as 2D shapes, and a PC-based 2D performance prediction model for such wheels. For these reasons, our study focused on a lugged wheel.

There are only a few published reports on the interaction between wheels and planetary terrain such as lunar regolith. Freitag *et al.* [4] investigated several flexible wheels of different tread patterns for the Apollo Lunar Roving Vehicle (LRV) and reported that a uniform or near-uniform distribution of contact pressure was desirable and they found no particular advantage in reducing the contact pressure below 3.45 kPa for their tested flexible wheels. Moreover, the performances of several LRV wheels were reported by using a single-wheel dynamometer system and a wheel with 50% covered tread pattern showed slightly superior performance in Lunar Soil Simulant test [5]. Successively, two LRV wheels were tested to determine the influence of wheel speed, acceleration, travel direction, the presence of a fender, or wheel load [6]. LRV wheels were however much larger than those envisaged for our lunar micro rover. Their study of the wheel performance on a slope of prototype rover models used three metrics: the pull coefficient, torque coefficient, and the power number [4–6].

Moreover, the experiences of manufacturing of candidate wheels for Apollo LRV were recently reported, and the decision processes for selection of LRV wheels were summarized in detail [7]. The computational model NWVPM (Nepean Wheeled Vehicle Performance Model) was used to predict the mobility of various wheels for LRV, and its predictions were accurate within the range of soil conditions published in some reports [8].

For small wheels, Richter and Hamacher [9] attempted to simulate the locomotion performance of microrovers on the Martian surface for the European Space Agency (ESA) by applying Bekker's formula. They constructed a 19.2 cm diameter lugged rigid wheel, designed for a mobile instrument deployment device vehicle with a mass of 8.6 kg, that applies a load of 7.92 N per wheel. Richter *et al*. further developed a predictive wheel-soil interaction model for Mars rovers using Bekker's approach with a combination of the nonlinear slip-sinkage relationship and the contact area based modification of the shear deformation modulus K [10]. Their modified model became sufficiently accurate to predict the performance of the Solar Powered Exploration Rover (SOLERO) and JPL Mars Exploration Rover (MER) wheels on DLR Mars Soil Simulant C (MSS-C) soil.

Recently, experimental approaches to wheel performance on sloped terrain have been developed using a sloped test bed with a lunar regolith simulant. A possible star shaped wheel with specially arranged lugs was reported, but a detailed evaluation of power consumption was not included [11]. Moreover, a specially designed small elastic wheel demonstrated superior performance to the rigid lugged wheel [12].

The discrete, or distinct, element method (DEM), initially proposed by Cundall [13], has become popular as a computational tool for dynamics of particles or powders in science and engineering. In the assembly of particles, there should be some effects of the potential forces from ambient particles other than the locally contacting. However, the present computational capability is still limited in considering all such forces. Thus, in DEM, the local contact reaction of two contacting elements is only considered.

In principle, DEM is based on the equation of motion, where all forces (such as contact reaction and body force) acting on the element of interest are added to the force term. After calculating all forces for all elements, the equations of motion are integrated to obtain subsequent velocities and displacements. The DEM solution is generally based on an explicit integration whose stability is conditional [13], which implies that the time step should be as small as possible. Moreover, for stable analysis, there exists the allowable range of time step in terms of the computational cost.

The normal contact reaction is calculated by contact models, such as the linear spring model [13] and Hertz contact model [14]. Similarly, both the linear spring model [13] and Mindlin-Deresiewicz contact model [15] are applied in calculating the tangential contact reaction. Viscous reaction forces are also assumed in both the normal and tangential directions. The shape of discrete elements can freely be defined, but simple shapes, such as a circle for 2D, or sphere for 3D, are most popular in terms of the detection of contact [13]. Other elemental shapes, such as an ellipse [16], polygon [17], or a clump of two or more circles [18] have also been applied in 2D DEM in the past.

Although a strict analysis of DEM based on the real element radius of soil particles might be ideal [19], at present, the radius of the element can not be of the same order as that in the target soil particles because of the computational cost. In this sense, the DEM element is a virtual element with a representative element radius that is larger than the real soil particles [20]. Therefore, the parameters used in the contact model of DEs should be determined or calibrated with comparative experiments using similar particle conditions.

Off-road wheel performance could be analyzed with sufficient accuracy [3, 18, 19, 21–25] by DEM. Furthermore, the performance of a lugged wheel on a horizontal lunar terrain could be predicted by simply reducing the gravity from 1 to 1/6 G, while holding other DEM parameters–such as spring constants and damping coefficients–constant [24, 25]. Using ellipsoid for soil elements, application of 3D DEM to the wheel of the MER under various gravities was recently reported [26]. The results indicated that the wheel torque increased almost linearly with gravity. The authors' group verified the use of constant DEM parameters in low gravity conditions through analysis of sand pile formation under low gravity by performing a DEM simulation and airplane experiments [27]. Note that the analysis of DEM for

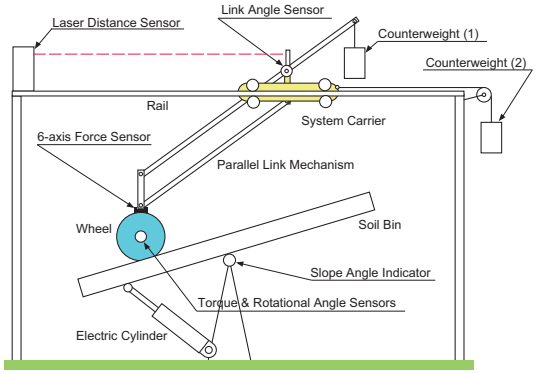

Fig. 1. Schematic diagram of the sloped soil bin and single wheel dynamometer

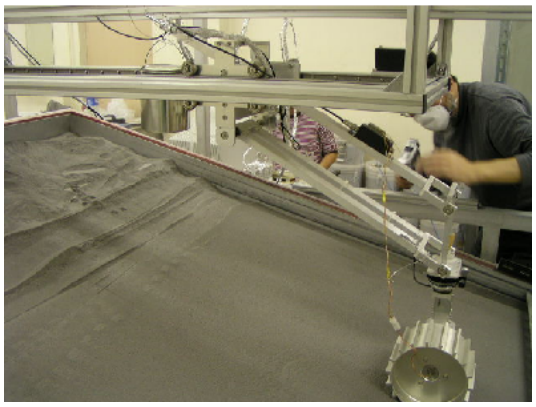

Fig. 2. View of the soil bin and single wheel dynamometer

sand pile formation under lunar gravity conditions was also reported but there was no comparison with experimental results [28].

The purpose of this study is to analyze the performance of a lugged wheel for a lunar micro rover on sloped terrain using the 2D DEM procedure previously developed for horizontal terrain [24]. The analysis accuracy will be confirmed by experiments using a sloped test bed. The parameters for the lugged wheel are numerically investigated in terms of metrics, such as slope angle for 20% slip and power numbers, and a candidate wheel configuration is selected. Moreover, wheel performance on a sloped lunar terrain is predicted by DEM analysis with reduced relative gravitational acceleration using the selected lugged wheel configuration.

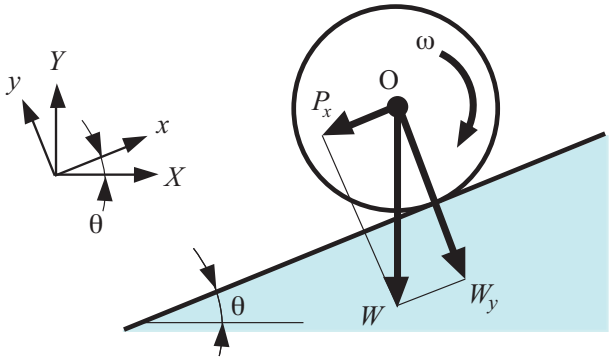

Fig. 3. Wheel travel on a slope

2 Experiments with single wheel performance on the slope

2.1 Sloped soil bin with a single wheel dynamometer

A sloped mobility test bed, consisting of a wide soil bin with effective inner dimensions of 1.5 m (width), 2.0 m (length), and 0.2 m (depth), which could be tilted, was constructed at Chofu Aerospace Center (CAC), JAXA [29]. The soil bin is axially rotated using a linear electrically driven actuator. A schematic configuration of the experimental facility is shown in Fig. 1.

A horizontal frame of the wheel carrier was constructed over the sloped soil bin. A target wheel attached at the end of a parallel link mechanism can freely sink vertically, with its weight controlled by the counterweight (1). Another counterweight (2) is adjusted to counteract the motion resistance of the system carrier so that the applied drawbar condition can be controlled properly. A six axis force sensor monitors the motion resistance by measuring the horizontal reaction. The vertical sinkage of a wheel is measured indirectly with a rotation angle sensor as the difference in the angle at the hinge point of the parallel link mechanism. Finally, a laser distance sensor monitors the horizontal travel distance of the wheel. Figure 2 shows a photo taken during the experiment.

Figure 3 shows the climbing wheel motion on sloped terrain with slope angle θ. While we define the conventional global coordinate system (X, Y), the local coordinate system of (x, y) is defined such that the x-axis is taken along the sloped surface as shown in Fig. 3.

In this simulation of wheel travel on a slope, the inputs are slope angle θ, constant wheel rotation velocity ω, and vertical contact load of the wheel W. In accordance with wheel dynamics over soil elements under contact, the wheel travels over the soil surface with the local travel velocity V_s, which can be calculated with respect

to a unit time step of numerical integration as

$$V_s = V_X \cos\theta + V_Y \sin\theta \tag{1}$$

where V_X is the horizontal travel velocity, V_Y is the vertical velocity, and θ is the slope angle. Note that V_X can be obtained from the distance signal of the laser distance sensor, and V_Y is calculated using the output from the angle sensor of the parallel link rotation in the experiment (see Fig. 1).

The slip i of a wheel can then be expressed using V_s such that

$$i = 1 - \frac{V_s}{r_w \omega} \tag{2}$$

where r_w is the free rolling radius of the wheel, assumed as the outer radius of the wheel $D/2$ including lug height L_H, since the measurement of free rolling radius is difficult for relatively soft soil conditions as in this study.

The pull coefficient is defined as the ratio of drawbar pull P_x to the vertical contact load of wheel W, i.e., P_x/W. As shown in Fig. 3, the pull coefficient is not a performance variable but a state variable, which can be expressed as $P_x/W = \sin\theta$ for sloped terrain locomotion. The torque coefficient can be expressed as the ratio of wheel torque T to a product of the vertical contact load W and the rolling radius of the wheel r_w, i.e., T/Wr_w. The power number PN measures the power consumption per unit of distance per unit of wheel weight in the locomotion from the starting point to the end point, and can be defined as follows [4]:

$$PN = \frac{T\omega}{WV_s} \tag{3}$$

A wheel performs better if the torque coefficient decreases and if the power numbers decrease.

2.2 Wheel specifications

Various test wheels made of aluminum were used in the experiments [23,24]. Their specifications are summarized in Table 1, where D is the total wheel diameter, D_0 is the rim diameter without lug, B is the width of the wheel, L_H is the height of the lugs, L_T is the thickness of the lugs, and L_n is the total number of lugs per wheel. The coefficient C_l represents the percent cover of the wheel lugs such that:

$$C_l = \frac{A_l}{A_w} = \frac{L_n B L_T}{\pi B D_0} = \frac{L_n L_T}{\pi D_0} \times 100(\%) \tag{4}$$

Table 1
Wheel specifications for slope locomotion

Wheel No.	D(mm)	D_0(mm)	B(mm)	L_H(mm)	L_T(mm)	L_n	C_l(%)
1	220	200	50	10	5	18	14.3
2†	220	200	100	10	5	18	14.3
3	220	200	150	10	5	18	14.3
4	170	150	100	10	5	18	19.1
5	270	250	100	10	5	18	11.5
6	210	200	100	5	5	18	14.3
7	220	200	100	10	5	36	28.6
8	240	200	100	20	5	18	14.3
9	220	200	100	10	10	18	28.6

†Wheel No. 2 is the base condition of reference.

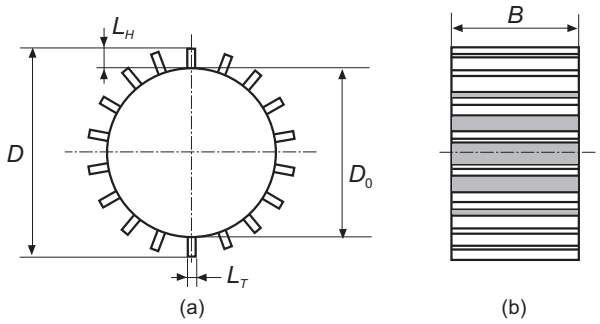

Fig. 4. Lug parameters

where A_w is the area of possible contacting surface of wheel rim, and A_l is the total section area of lugs .

The definition of lug parameters is shown in Fig. 4; Fig. 4(a) shows the wheel side view, and Fig. 4(b) shows the front view of a wheel with width B.

2.3 Experimental conditions

In the experiment, a lunar regolith simulant, FJS-1, prepared by Shimizu Corporation, was used to fill the soil bin to a depth of 10 cm, which was the same depth as in previous experiments on horizontal terrain [3,23]. Since the data of in situ observation in the Apollo 15 mission [30] indicated that there might be a relative density layer of very dense (hard) in lunar terrain around a depth of 10 cm or more, the depth of the simulant in the experiments was set to 10 cm, which assumes the existence of hardpan below 10 cm. The physical properties of FJS-1 are summarized

Table 2
Physical property of lunar regolith simulant FJS-1

Specific gravity of particle	2.94
Minimum bulk density ρ_{min} (g/cm^3)	1.4
Maximum bulk density ρ_{max} (g/cm^3)	2.0
Cohesion c (kPa)	2.55
Angle of internal friction ϕ (deg)	37.2

Table 3
Experimental conditions

Vertical wheel load W (N)	9.8, 14.7, 19.6
Slope angle θ (deg)	0, 10, 15, 20, 25
Angular velocity of wheel ω (rad/s)	0.1, 0.2, 0.3

in Table 2 [29].

Before each experiment, the simulant was manually raked and moved up and down within the soil bin and leveled with a leveling plate. The dry bulk density ρ_d in the experiments were monitored frequently by a vane shear device at three locations on the soil surface. The obtained shear torque was converted to ρ_d based on the calibration, which represented the value of ρ_d at a depth of 4 cm. Throughout the experiments, the average of ρ_d was found to be 1.48 g/cm^3. The relative density D_r can then be calculated by

$$D_r = \frac{\rho_{max}}{\rho_d}\left(\frac{\rho_d - \rho_{min}}{\rho_{max} - \rho_{min}}\right) \times 100(\%) \tag{5}$$

From Eq. (5), D_r could be experimentally obtained as 17.4%. Note that this relative density condition is classified as “loose” [4, 30].

Shear strength parameters of FJS-1, such as cohesion and angle of internal friction, were obtained by conventional triaxial compression test with confining pressures similar to the reported measurement for JSC-1 [31]. Cohesion is thought to be related to inter particle attractive force, which becomes dominant for particles of smaller diameter [29].

Experiments were conducted using the conditions listed in Table 3. The vertical contact load contains the wheel weight. Experiments were repeated twice under the same conditions.

In the numerical simulation, the vertical contact load W was held constant for all slope angles, as was done in the experiment. The drawbar load P_x is applied as the slope angle θ is changed, based on the relationship of $P_x = W \sin\theta$. The ratio of

Table 4
Variation of ratio of P_x/W on the slope

θ (deg)	P_x/W
0	0.0
5	0.0872
10	0.1736
15	0.2588
20	0.3420
25	0.4226

$P_x/W(= \sin\theta)$ is summarized in Table 4. Acceleration forces are assumed to be negligible in the table.

3 DEM analysis of lugged wheel performance for sloped terrain

We previously reported the applicability of DEM for analyzing tractive performance of rigid lugged wheels for a lunar microrover on horizontal surfaces [23,24]. The analysis of wheel performance by DEM for various slopes is summarized in this section.

3.1 Outline of analysis

Since the computational cost is still high in the application of 3D analysis, this study applied 2D DEM. The parameters for contact reaction are the spring constant, the viscous coefficient in normal and tangential directions, and the friction coefficient. This study uses a trial-and-error approach for an initial parameter guess, as in the previous study [24]. The justification of the selected parameter values is then verified by comparing the DEM with experimental results, as shown in Section 4.

Small DEM elements, embedded virtually at lug positions, are used for the contact check and contact reaction calculation between wheel lugs and soil [24]. All reactions from lug elements are added as the reaction of the wheel element.

Other small virtual DEM elements are embedded in three walls–two sides and one bottom–of the soil bin to facilitate the generation of sloped terrain conditions. These virtual wall elements are used only for contact calculation at the soil bin walls, and they do not move or rotate from contact reaction.

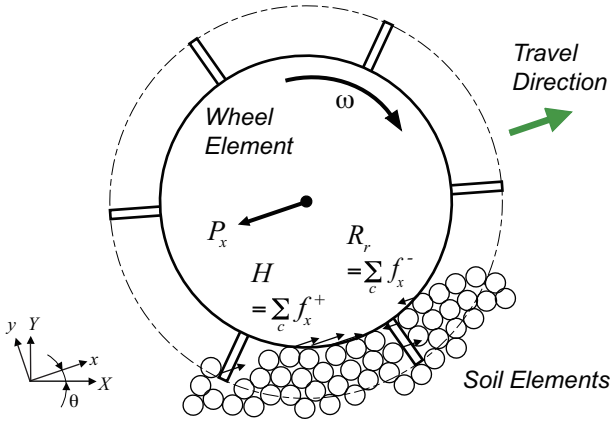

Fig. 5. Tractive effort and motion resistance on the slope for DEM

3.2 *Wheel performance analysis on the slope*

Each x-component of the contact reaction force f_x on a wheel and lug element is summed to obtain either the calculated gross traction H (if $f_x \geq 0$), or motion resistance R_r (if $f_x < 0$), with respect to the local x-axis as shown in Fig. 5.

After obtaining the gross traction H and the motion resistance R_r with DEM, we calculate the net traction P_d using $P_d = H - R_r$ with respect to the local x-coordinate axis on the slope.

3.3 *Preparation of DEM simulation*

The parameters used in DEM analysis are summarized in Table 5. Note that the density of the regolith element of 1.55 g/cm^3, which corresponds to the value of the bulk density at about 5 cm below the lunar regolith surface [30], is used for calculating the damping coefficient.

The elemental density ρ (g/cm^3) was calculated based on the initially generated depth of the regolith element Z_e using the following empirical relation from the Apollo program [30]:

$$\rho = 1.89 \times \frac{Z_e + 1.69}{Z_e + 2.9} \tag{6}$$

where Z_e is the depth of lunar regolith element (cm).

The spring constants (K_n, K_t) were initially set to the same values as in the previous study on wheel performance on horizontal terrain [23, 24]. The friction coefficient between soil DEs μ is from the angle of internal friction of FJS-1. Friction coefficient of the soil bin walls μ^w is set by assuming the composition of wall to be

Table 5
Parameters in DEM simulation

Number of elements for regolith	6986
Diameter of the regolith element, *random* (mm)	2.8, 3.2, 3.6, 4.0
Regolith elemental density (g/cm^3)	1.55†
Mass of the wheel (g)	500
Diameter of the lug element (mm)	2.5
Diameter of the wall element (mm)	2.5
Slope angle θ (deg)	0, 5, 10, 15, 20, 25
Vertical contact load W (N)	9.8, 14.7, 19.6
Drawbar load P_x (N)	$W \sin\theta$
Angular velocity of the wheel ω (rad/s)	0.138
Duration of soil consolidation (s)	1.0, 6.0
Duration of vertical sinkage (s)	1.0
Simulation time for wheel travel (s)	40.0
Time step increment (s)	0.00005
Normal spring constants K_n, K_n^w and K_n^L (N/m)	10,000
Tangential spring constants K_t, K_t^w and K_t^L (N/m)	500
Friction coeff. between regolith elements μ	0.75
Friction coeff. for wall contact μ^w	0.75
Friction coeff. for wheel contact μ^L	0.5

† This density value is used for damping coefficient calculation.

soil, while that for the wheel and lug contact μ^L is the same as in the previous study. Damping coefficients were calculated using the critical damping formula, such that $C_n = 2\sqrt{m_e K_n}$ for a normal damper and $C_t = 2\sqrt{m_e K_t}$ for a tangential damper, where m_e is an equivalent mass representatively calculated by using ρ = 1.55 g/cm^3, B and r_{max}.

Moreover, in Table 2, the lunar regolith simulant FJS-1 shows cohesion as well as internal friction. As reported in our previous studies [23, 24], DEM results showed sufficient accuracy when compared with the experimental result, although the effect of cohesion was not explicitly introduced in the contact model in our DEM analysis. The introduction of cohesive reaction in a DEM contact model can easily be realized by an additional parallel tensile spring model [32], or an internal locking force model [33].

In the preliminary DEM analysis, the wheel rotational velocity did not exhibit a

significant effect on wheel performance parameters, such as slip, gross traction, and net traction. Thus, the data from the previous paper [24], of ω = 0.138 rad/s, is used in the analysis unless otherwise stated. Table 1 also lists the parameters for lug configuration and wheel diameter used in DEM.

DEM simulation for wheel performance is divided into four stages: (i) initial soil consolidation by their own weight of elements with the horizontal soil bin; (ii) rotation of the soil bin to the required slope angle; (iii) secondary consolidation with free wheel sinkage on to sloped soil surface and (iv) wheel travel simulation on sloped terrain [23].

In the first stage, the preparation of soil discrete elements is performed by analyzing the consolidation of soil DEs with their own weight of the elements from the initial regular configuration of DEs in the soil bin. The preparation of the soil condition in the experiment, however, involves manual mixing of the simulant with a hand rake, and leveling the disturbed surface by sliding a leveling blade over the edge of the soil bin. However, the present 2D DEM cannot include such preparation procedures due to computational cost as well as the limited degrees of freedom of the analysis.

At the wheel travel stage, the wheel sinkage was calculated as the local average sinkage z_a from the reference where the wheel begins to rotate. This avoids the difficulty of defining zero wheel sinkage with various lug conditions running over the uneven sloped surface of random soil DEs.

4 DEM analysis results and comparison with experimental results

4.1 Relationship of slope angle and slip

The specific wheel condition of D_0 = 200 mm, B = 100 mm, and W = 14.7 N was selected for calibration of DEM analysis so that the selected DEM parameters could be verified sufficiently to obtain comparable results from experiments.

Figure 6(a) shows the result of a wheel with L_H = 10 mm and L_n = 18. A large difference between DEM analysis and experiments can be seen at a slope of 15 deg, where the slip difference reaches 20%. Figure 6(b) indicates a smaller wheel slip with L_H = 20 mm and the same L_n = 18 at a slope of 25 deg in both DEM analysis and experiments. The largest slip difference between DEM and experiments is 16.3% at a slope of 20 deg. In Fig. 6(c), DEM and experimental results show similar behavior, but the difference in slip becomes large at the slope angles of 15 and 25 degrees in the experimental results. Comparing experimental results with numerical ones in Fig. 6, it can be stated that the selected parameters listed in Table 5 are sufficient for the DEM analysis of wheel performance on sloped terrain.

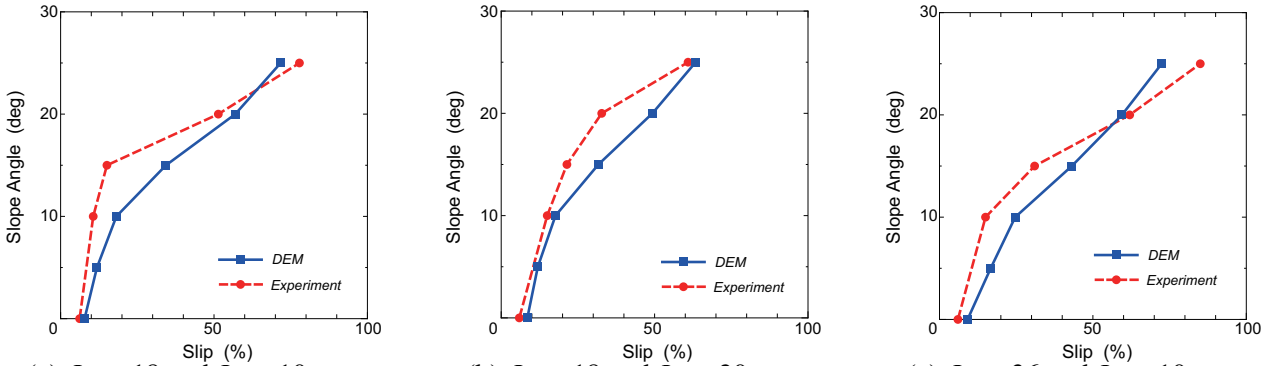

(a) L_n = 18 and L_H= 10 mm (b) L_n = 18 and L_H= 20 mm (c) L_n = 36 and L_H= 10 mm

Fig. 6. Result of slip and slope (1)

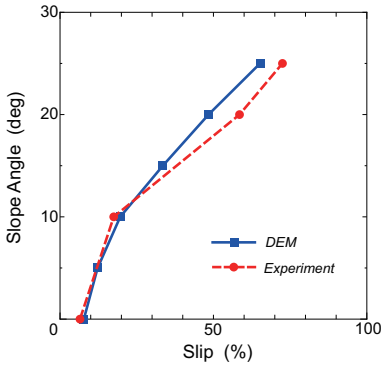

Fig. 7. Result of slip and slope (2)

To further verify the performance of DEM, a wheel with a larger vertical contact load of W = 19.6 N with L_H = 20 mm and L_n = 18 was analyzed and the result of DEM was compared with recent experimental results [12], as shown in Fig. 7. The figure clearly indicates that the current DEM analysis can be applied with sufficient accuracy over a wide range of experimental conditions.

4.2 Relationship of slope angle and wheel sinkage

Experimental results for the wheel with L_H = 20 mm and L_n = 18 for slopes of 10, 15, 20, and 25 deg are shown in Fig. 8. The straight solid lines indicate the ideal slope lines for the given caption: blue for 10 deg, green for 15 deg, purple for 20 deg, and red for 25 deg. It is clear that the wheel on a 25 deg slope travels with significant wheel slip and sinkage; the wheel travel is equivalent to that over the terrain with a slope of 20 deg. The DEM result (dashed lines) also indicates a similar reduction in wheel travel equivalence from 25 deg to 20 deg, as shown in Fig. 8. Other wheel conditions, such as L_H = 10 mm and L_n = 36, showed a similar equivalence in the results of experiments and DEM to that seen in Fig. 8. Thus, a slope of 20–25 deg might be the maximum for wheel locomotion.

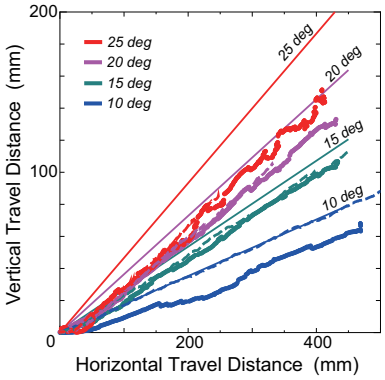

Fig. 8. Experimental and numerical wheel sinkage on sloped terrain

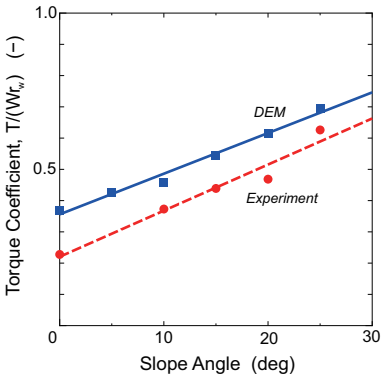

Fig. 9. Slope angle and wheel torque

4.3 Relationship of slope angle and wheel torque

Figure 9 shows the relationship between the slope angle and torque coefficient. The wheel is $D_0 = 200$ mm, $L_H = 20$ mm, $L_n = 18$, $B = 100$ mm, and $W = 14.7$ N. DEM analysis obtains the wheel torque T as $T = Hr_w$, where H is the gross traction, and r_w is the freely rolling radius of the wheel, which is assumed to be $r_w = D/2$. The torque coefficient is then calculated as $T/(Wr_w) = (Hr_w)/(Wr_w) = H/W$. In DEM, the wheel torque may be obtained directly from the wheel contact reaction. However, the DEM program in this study shares a common subroutine for contact reaction with that in our previous study [24]. Therefore, this study does not use the wheel torque directly obtained at the wheel element. The torque coefficient obtained by DEM analysis overestimates the experimental result by as much as of 0.15, although both show a similar linear increase with respect to the slope angle.

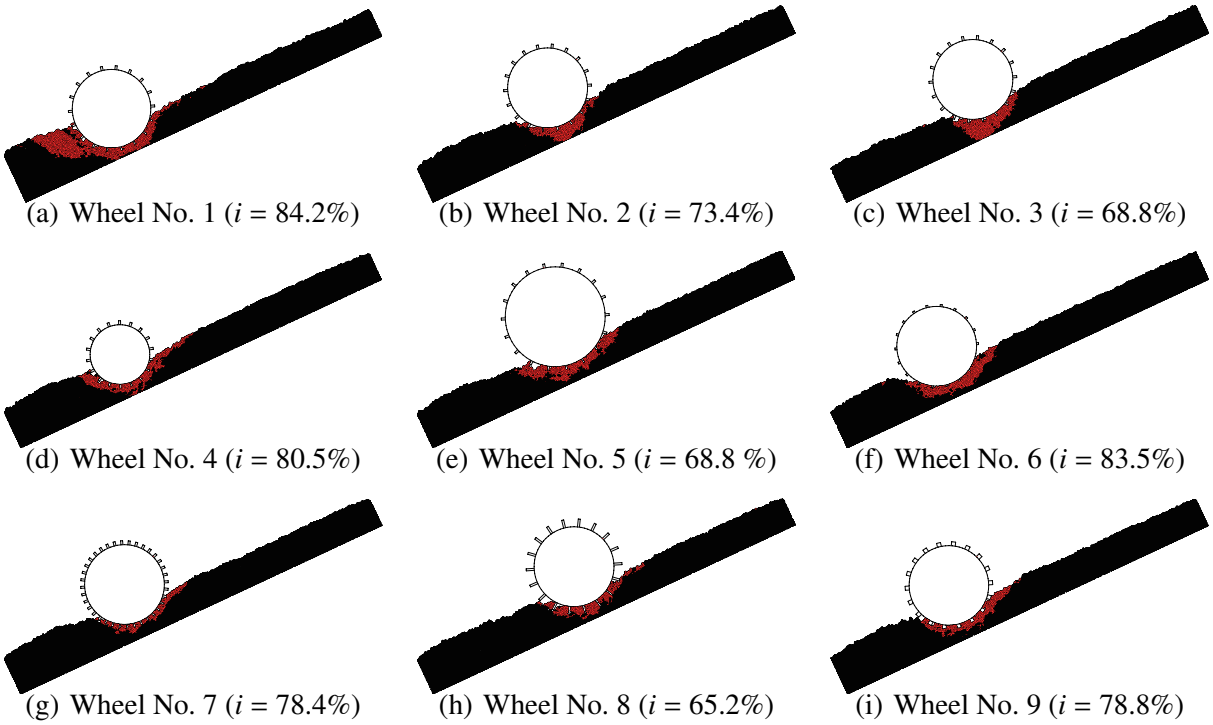

(a) Wheel No. 1 (i = 84.2%) (b) Wheel No. 2 (i = 73.4%) (c) Wheel No. 3 (i = 68.8%)

(d) Wheel No. 4 (i = 80.5%) (e) Wheel No. 5 (i = 68.8 %) (f) Wheel No. 6 (i = 83.5%)

(g) Wheel No. 7 (i = 78.4%) (h) Wheel No. 8 (i = 65.2%) (i) Wheel No. 9 (i = 78.8%)

Fig. 10. Instantaneous soil flow under a wheel on 25-degree slope

5 Parametric investigation of lugged wheel performance on a sloped terrain by DEM

5.1 Remarks on soil flow under a wheel

Figure 10 shows the DEM result of instantaneous soil flow on 25-degree slope for each wheel in Table 1. The red region expresses the soil elements whose displacement becomes larger than 1 mm within a time step of 0.1 sec. Comparing the results for wheel numbers 1 to 3 [Figs. 10(a) to (c)] clearly shows that an increase in wheel width contributes to the prevention of sinkage. Moreover, the red region, indicating the area activated by lugs, clearly did not extend widely but remained close to the lug area in Figs. 10(g) to (i). Because of the effect of soil flow between or under the wheel lugs and the induced instability of soil with respect to internal friction angle, the figure shows that the soil element in front of the wheel flows by itself. Note that similar activated region with slip is seen in Figs 10(g) and 10(i) at the same coefficient of C_l = 28.6% for D_0 = 200 mm.

With respect to the bottom baseline of soil bin, an outline of mobilized zone of soil reaches to the bottom and is distorted in case of wheel number 1 because of the increased slip and sinkage of the wheel as seen in Fig. 10(a). Other wheels would not suffer significant effect of bottom wall of soil bin in terms of their outline shapes. For the effect of different diameter of wheel, wheel number 4 with small diameter

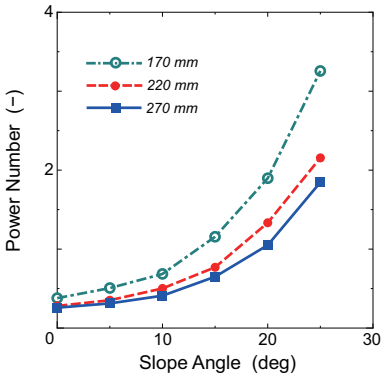

Fig. 11. Effect of the wheel diameter on the power number

[Fig. 10(d)] shows large sinkage, while wheel number 5 with large diameter [Fig. 10(e)] portrays small sinkage. The outline of mobilized zone under wheel number 5 expands widely, and that for wheel number 4 also grows wide under the wheel, because of increased slip and sinkage. On the other hand, wheel number 7 with L_n = 36 [Fig. 10(g)] shows the smallest mobilized zone of soil in all wheel conditions, caused by the action of densely distributed lugs.

5.2 *Effect of the wheel diameter on the power number*

Figure 11 shows the effect of the wheel diameter D on the PN, with DEM result for wheels with D_0 = 150, 200, and 250 mm; L_H = 10 mm; L_n = 18; B = 100 mm; and W = 19.6 N. In DEM, the circumferential velocity at the end of the lug was kept constant at 1.52 cm/s by adjusting the angular velocity ω to observe the geometrical effect of the wheel diameter.

For the largest difference in PN at a slope of 25 degrees, each DEM result is summarized as follows: the gross traction for cases of D_0 = 150, 200, and 250 mm is 12.45, 11.25, and 10.78 N respectively. Similarly, the running resistance is 4.15, 2.94, and 2.48 N respectively. Moreover, the average sinkage is 2.04, 1.71, and 1.53 cm respectively. Thus, it is understood that, since a larger wheel diameter increases the contact area of the wheel under the same vertical contact load W and net traction P_d, wheel sinkage would be reduced, resulting in a smaller rolling resistance and slip at larger slope angles.

5.3 *Effect of wheel load on the power number*

The simulation result for a wheel when W = 9.8, 14.7, and 19.6 N; L_n = 18; D_0 = 200 mm; B = 100 mm, is shown in Fig. 12. In Fig. 12(a), L_H=10 mm, and in Fig. 12(b), L_H= 20 mm.

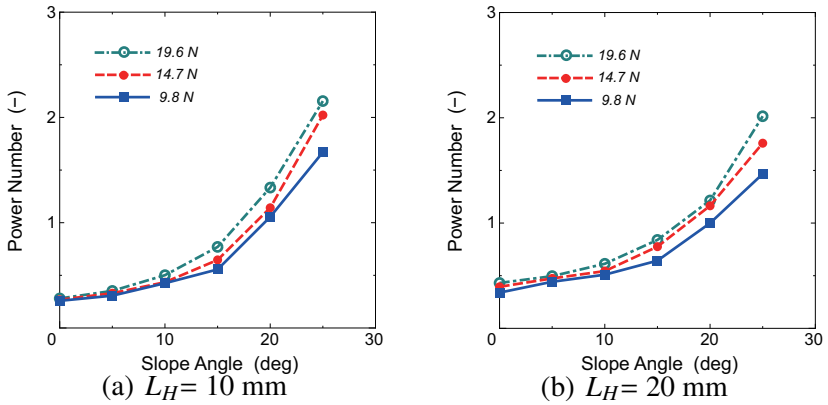

(a) L_H= 10 mm (b) L_H= 20 mm

Fig. 12. Effect of wheel load on the power number

It is evident that the *PN* is reduced if the wheel load is low. For example, for the 25 degree slope shown in Fig. 12(a), the average sinkage z_a and the running resistance R_r were 1.18 cm and 1.46 N for W = 9.8 N, 1.59 cm and 2.18 N for W = 14.7 N, 1.71 cm and 2.94 N for W = 19.6 N. However, the ratio of H/W , i.e. the torque coefficient as stated in 4.3, remained almost constant at 0.572–0.574. The low contact load W results in small wheel sinkage for a given slope, which contributes to the low running resistance R_r. The low running resistance implies low wheel slip, which reduces the *PN*. The difference in *PN* for 14.7 N and 19.6 N decreases at a slope of 20 deg. Moreover, at slope angles of 0 and 5 deg, the *PN* difference for various W also decreases.

5.4 Effect of wheel width on power number

Figure 13 summarizes the simulation result for wheels with B = 50, 100, and 150 mm; L_H = 10 mm; L_n = 18; D_0 = 200 mm; and W = 19.6 N. The figure shows the effect of wheel width B on the *PN*. In all cases, if the wheel width increases, the *PN* decreases because of reduced wheel sinkage, reduced running resistance, and, therefore, of reduced wheel slip, as i = 84.2% for a 50-mm-wide wheel and i = 68.8% for a 150-mm-wide wheel. Note that the difference in *PN* between widths of 100 and 150 mm is not as large as the difference between 50 and 100 mm, when L_n = 18 [Fig. 13(a) and (b)]. Among the three wheel conditions, a wheel with L_n = 18, L_H = 10 or 20 mm would be effective in terms of a low *PN*. From the figure, it is evident that the effect of wheel width may not be linear for some given slope angles and that an optimum wheel width may exist. The latter is due to increasing motion resistance from bulldozing for increased wheel width, offsetting the reduced sinkage.

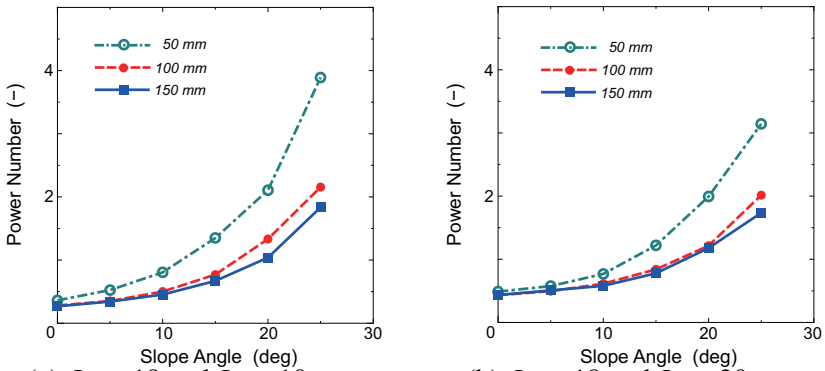

(a) L_n = 18 and L_H= 10 mm (b) L_n = 18 and L_H= 20 mm

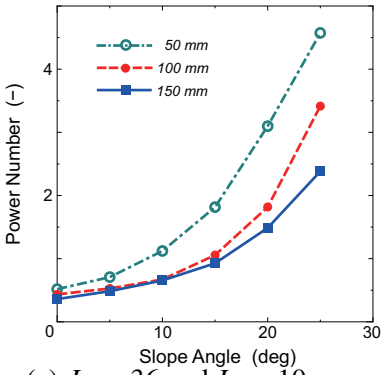

(c) L_n = 36 and L_H= 10 mm

Fig. 13. Effect of wheel width on the power number

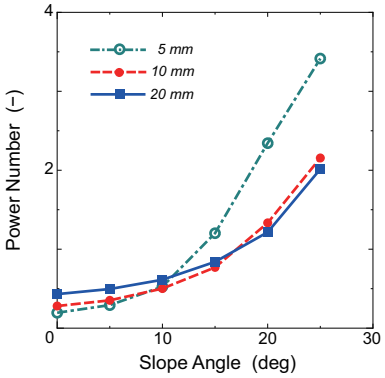

Fig. 14. Effect of lug height on the power number

5.5 *Effect of lug height on the power number*

Figure 14 illustrates the effect of lug height on the *PN* for L_n = 18, D_0 = 200 mm, and W = 19.6 N. The *PN* curve is lower for a lug height of L_H = 10 or 20 mm, clearly showing that a higher lug height may be more effective for slope locomotion.

In Fig. 14, it is noted that the curve for lug height of L_H = 20 mm indicates largest power number among three lug height conditions for smaller slips below or equal

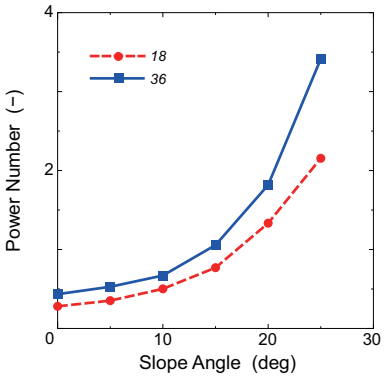

Fig. 15. Effect of lug number on the power number

to 10%. This would imply the possibility of trade-off between power consumption on horizontal terrain and that on sloped terrain for L_H = 20 mm.

A wheel with L_H = 20 mm [Fig. 10(h)] shows a narrow range of activated soil region that is mostly confined by the action of lugs within the outer most diameter of wheel D to create a clear line of shear. For wheels with smaller lug height [e.g. Fig. 10(f)], although the zone of mobilized soil extends outside of D, the soil around the wheel also becomes activated and the wheel itself does not generate larger gross traction through the action of its lugs because of the reduced friction coefficient of 0.5 between the lug or wheel rim and soil elements; this increases wheel slip and thus the power number.

5.6 Effect of the total numbers of lugs on the power number

Figure 15 shows the simulation result for a wheel with L_n = 18 and 36 while using L_H = 10 mm, D_0 = 200 mm, W = 19.6 N, L_T = 5 mm, and B = 100 mm. The effect of the number of lugs on the PN is clearly seen–the wheel with L_n = 18 has a better PN than that with L_n = 36.

To rationally describe the contributing mechanism of total number of lugs L_n, the coefficient C_l of different wheels is compared. From Table 1, the coefficient C_l for wheel number 2 is 14.3%, while that for wheel number 7 is 28.6%. In terms of the effect of the total number of lugs, a larger coefficient C_l means that the ratio of the soil part within the contact area of wheel becomes small. However, the lug faces, acting as a soil cutting tool, generate the gross traction in a lugged wheel. Moreover, the bottom lug face contributes to soil compaction that affects the wheel running resistance. From these conditions, the result of gross traction for wheel number 7 becomes H = 14.45 N while generating R_r = 6.14 N as a negative effect. Thus, by cancelling the benefit of gross traction with running resistance under a small ratio of soil, the wheel with L_n = 36 displayed a lower performance in terms of its PN.

Within the combination of investigated parameters, a larger wheel with fewer lugs

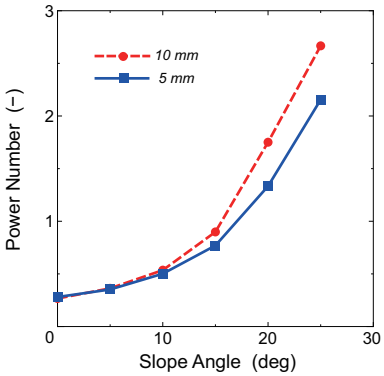

Fig. 16. Effect of the lug thickness on the power number

(e.g., D_0 = 250 mm and L_n = 18) may be suitable for a lunar micro rover in terms of the total wheel mass. Note that when the wheel diameter increases, e.g., to 300 mm, the effect of the number of lugs on the PN may differ, since the number of lugs within the contact area under the wheel will be small for L_n = 18.

5.7 *Effect of the lug thickness on the power number*

Figure 16 shows the simulation result for a wheel with L_n = 18, L_H = 10 mm, D_0 = 200 mm, W = 19.6 N, B = 100 mm, when the lug thickness is either L_T = 5 or 10 mm. It is clear that the effect of thickness on the PN is almost the same for slope angles up to 10 degrees. For slope angles steeper than 10 degrees, a wheel with L_T = 5 mm shows better performance in terms of the PN, but the difference in PN for a slope of 25 deg might be not so large, since there is only a slight difference in coefficient C_l and of wheel slip, which would contribute to the difference, and other factors, such as the average sinkage, gross traction, and running resistance, had almost the same values for two values of L_T. The coefficient C_l = 28.6% for L_T = 10 mm is the same as that for the wheel with L_n = 36 (wheel number 7 in Table 1), and the wheel might become similar to a wheel with almost no lug effect. For such cases, the generation of gross traction in DEM may depend on the friction coefficient μ^L between the wheel and soil rather than the friction coefficient μ between soil DEs.

5.8 *Remarks on lug parameters in relation with metrics*

From the parametric observations in this section, the effect of the lug parameters are summarized in Table 6, using the representative metrics for wheel performance, such as $\theta_{20\%}$, PN_{SP}, PN_{15deg} and $PN_{20\%}$ [4] for each wheel under W=19.6 N.

For slope angle at 20% slip ($\theta_{20\%}$) , the wheel performance is regarded as better if its angle increases. For other metrics , the wheel has better power consumption, if

Table 6
Representative metrics with superiority weight

Wheel No.	$\theta_{20\%}$ (deg)		PN_{SP}		PN_{15deg}		$PN_{20\%}$		Sum of weights
1	0.49	8	0.363	6	1.350	9	0.376	2	(25)
2	7.10	3	0.280	5	0.790	3	0.414	4	15
3	10.0	1	0.268	4	0.670	2	0.453	6	(13)
4	3.70	6	0.379	7	1.156	7	0.475	7	(27)
5	9.35	2	0.258	2	0.650	1	0.396	5	10
6	2.72	7	0.195	1	1.203	8	0.246	1	(17)
7	5.87	5	0.434	9	1.056	6	0.554	8	(28)
8	10.0	1	0.431	8	0.840	4	0.620	9	(22)
9	6.30	4	0.266	3	0.899	5	0.391	3	15
Average	6.17		0.319		0.955		0.436		

the PN decreases. An order of superiority is also shown by a simple integer for each metric, where a smaller number is input for higher performance. The last column in Table 6 summarizes the sum of four numbers, which implies the lowest sum might be regarded as the best wheel in terms of the four corresponding metrics. The sum with brackets indicates that some metrics in the table are out of the preferred range.

Comparing the metrics with respect to the corresponding average values shows that wheel numbers 2, 5 and 9 may be candidates for lugged wheels for the small lunar rovers under study. Wheel numbers 2 and 5 have similar lug parameters with different wheel diameters; D_0 = 20 cm for the wheel number 2 and D_0 = 25 cm for number 5. In terms of the smallest sum of weights, wheel number 5 may be a candidate wheel within the lug parameters investigated in this section. The selection of wheel number 5 may be the same result as in our previous DEM analysis on horizontal terrain [24]. Note that the diameter D of the wheel should be determined from other requirements, such as stowage of the rover vehicle in the lander.

The performance from DEM of a lugged wheel on a slope of 25 degrees, the result of tractive performance, such as gross traction H, net traction P_d, running resistance R_r and average sinkage z_a, which was integrated from the beginning of wheel rotation and end of wheel travel, is summarized in Table 7. The table verifies that wheel number 5 exhibits the best traction performance under the lug conditions examined, in terms of small running resistance and average sinkage. Wheel number 8 (L_H = 20 mm and L_n = 18) and wheel number 7 (L_H = 10 mm and L_n = 36) not only increased the gross traction but also increased running resistance while indicating the same average level of wheel sinkage.

It is noted that the effect of cohesion, which is not considered in the present DEM

Table 7
Performance of lugged wheel on 25-degree slope

Wheel No.	i(%)	H(N)	P_d(N)	R_r(N)	z_a(cm)
1	84.2	12.04	8.31	3.73	2.47
2	73.4	11.25	8.31	2.94	1.71
3	68.8	11.23	8.31	2.92	1.57
4	80.5	12.45	8.30	4.15	2.04
5	68.8	10.78	8.30	2.48	1.53
6	83.5	11.06	8.29	2.77	1.67
7	78.4	14.45	8.31	6.14	1.65
8	65.2	13.74	8.30	5.44	1.65
9	78.8	11.10	8.29	2.81	1.69

analysis, may become important in comparison of tractive performance of wheels with different contact areas as observed by z_a.

6 Prediction of lugged wheel performance on sloped lunar terrain

6.1 Introduction

The locomotion over lunar terrain has been a challenging topic for vehicle engineers ever since the US Apollo mission and the Luna mission of the USSR. The robotic rover Lunokhod 2 sank significantly in the vicinity of some craters, and the Apollo 15 LRV encountered isolated soft soil and became stuck [30]. Thus, predictions of wheel performance and the prospective rover design should take into account maneuverability in soft soil conditions.

The performance of a wheel on sloped lunar soft terrain is simulated using the selected wheel parameters (D_0 = 250 mm; B = 100 mm; L_H = 10 mm; L_T = 5 mm; L_n = 18) under a vertical contact load of W = 14.7 N. To observe the soil condition, the same contact load of W is used for both lunar terrain and earth terrain, which means the drawbar load P_x also becomes the same on the Earth and on the Moon depending on the slope angle.

Since adopting the same wheel contact load both for the Moon and Earth is expected to produce greater wheel sinkage, the initially generated thickness of soil DEs is increased to 15 cm, where the total number of soil DEs is 9980. Moreover, the length of the soil bin was extended, and for sloped terrain analysis the wheel was positioned in the middle of the soil bin to avoid the disturbance of soil flow

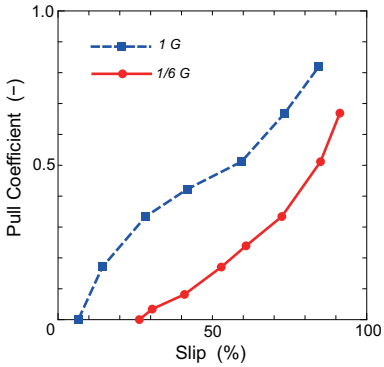

Fig. 17. Pull coefficient on horizontal terrain

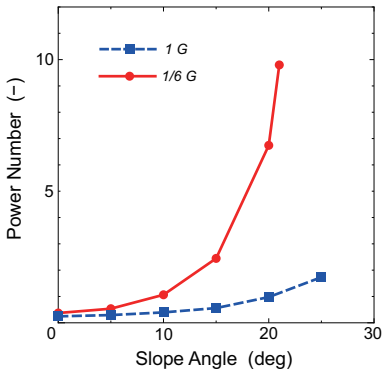

Fig. 18. Effect of gravitational acceleration on the power number

caused by its side walls. This produced a total of 15980 soil DEs for sloped lunar terrain analysis.

6.2 Pull coefficient obtained from the horizontal terrain condition

Firstly, the performance of wheel was obtained on the horizontal terrain. Various drawbar loads were input to simulate tractive performance of the wheel in 2D DEM [24]. The pull coefficient P/W at 1/6 G is shown in Fig. 17 along with the result at 1 G. From the figure, it is clear that the weak, or soft, condition of soil on the lunar gravity results in the increased sinkage of wheel and, thus, decreased output of pull coefficient. The slip of 26.3% for a zero pull coefficient at 1/6 G indicates reduced wheel mobility on horizontal lunar terrain.

6.3 Effect of gravitational acceleration on the power number

Figure 18 shows the PN under the effect of gravitational acceleration for slope locomotion. Note that the wheel cannot climb a slope of 25 degrees at 1/6 G. It is clear that the reduced gravity would increase the PN at all slope angles. The

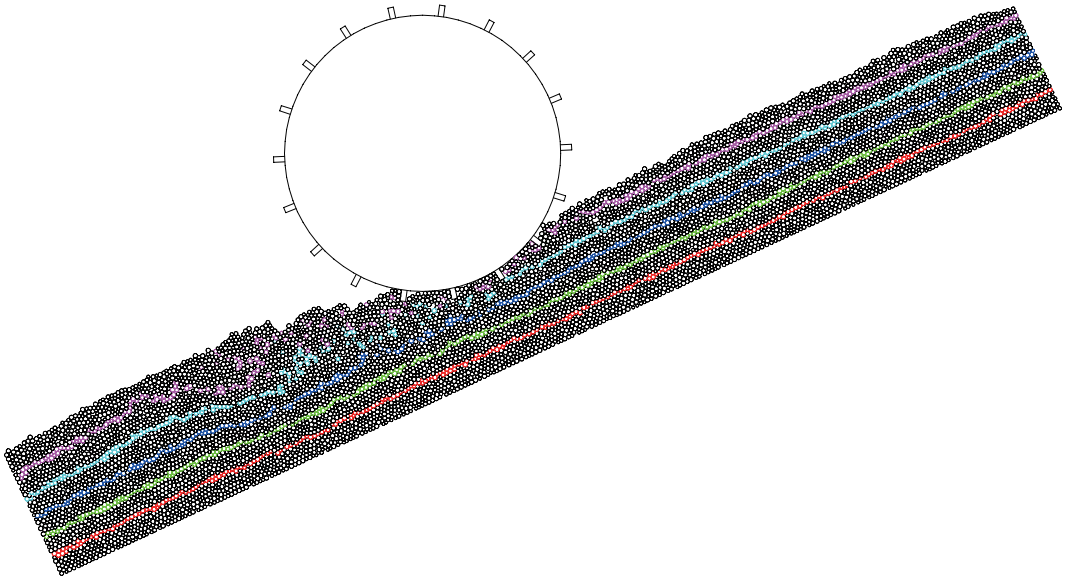

Fig. 19. Soil deformation under a wheel on a Earth slope of 25 degrees

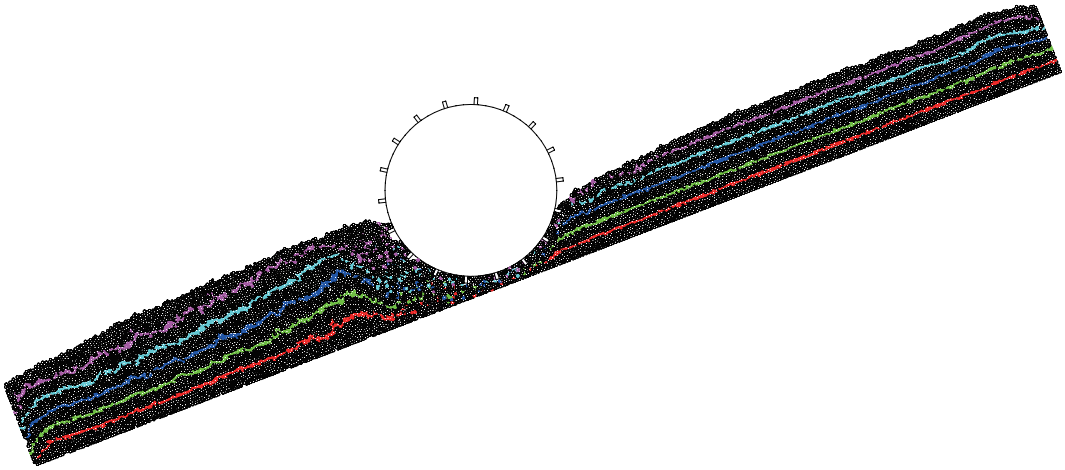

Fig. 20. Soil deformation under a wheel on a lunar slope of 21 degrees with extended soil bin condition

increased *PN*, especially for larger slope angles in the figure, implies an excessive energy expenditure due to the reduction of soil trafficability caused by reduced gravitational acceleration on the Moon.

6.4 Comparison of soil deformation under the wheel

Figure 19 shows the results of soil deformation for Earth gravity at a slope angle of 25 deg, where the wheel slip was 68.3%. The result of soil deformation for lunar gravity at a slope angle of 21 deg is shown in Fig. 20. In the figure, the slip was 94.4% at 1/6 G, and the wheel could not climb the slope angle at 25 deg as it did at 1 G. In both figures, the vertical contact load condition is the same.

The wheel sinks considerably with z_a = 3.01 cm at 1/6 G because of the increased slip, since the weight of the soil element would be reduced by 1/6, thereby reducing the compaction by its own weight even in the extended period of soil consolidation, as can be inferred from Fig. 20.

6.5 Discussion

It becomes clear that the candidate lugged wheel with D_0 = 250 mm, B = 100 mm, L_H = 10 mm, L_T = 5 mm, L_n = 18 under W = 14.7 N might have difficulty climbing a lunar terrain sloped more than 20 degrees. This is mainly due to the reduced trafficability of soil in a lunar environment.

Moreover, the preparation of the initial soil condition is an issue in application of the DEM. In the previous study [4], the following items were proposed for the experiments with simulants. Important parameters were relative density, cohesion, angle of internal friction, and penetration resistance gradient. Cohesion and the angle of internal friction can be regarded as input parameters in DEM, but the effect of cohesion is not yet implemented in our present analysis. The relative density and the penetration resistance gradient can be obtained as a result of the analysis, although our present DEM does not include these output.

The consolidation in the first stage of DEM analysis was thought to be a governing factor of soil conditioning on bulk density in low gravity conditions [27]. An inverse proportional factor of six was multiplied to the consolidation time of earth conditions to increase the duration of consolidation for lunar gravity of 1/6 G so that the soil DEs could be stabilized sufficiently by their own weight during consolidation. In the present analysis, however, the effect of extended time for lunar gravity could not be found because the initial generation of soil DEs was done in a rather dense configuration, where the fall height of each soil element could not be large. For the precise prediction of lugged wheel performance on the Moon, the preparation of initial condition of soil DEs should be investigated.

7 Conclusions

To confirm the applicability of DEM for sloped terrain locomotion, the relationships of slope angle with slip, wheel sinkage and wheel torque obtained by DEM, were compared with experimental results measured using a slope test bed consisting of a soil bin filled with lunar regolith simulant. Among the lug parameters investigated, a lugged wheel with D_0 = 250 mm, B = 100 mm, L_H = 10 mm, L_T = 5 mm, L_n = 18 was found, on average, to have excellent performance in terms of metrics, such as $\theta_{20\%}$, PN_{SP}, PN_{15deg} and $PN_{20\%}$. The estimation of wheel perfor-

mance over sloped lunar terrain showed an increase in wheel slip, and a possibility that the selected lugged wheel might not have locomotion on a slope greater than 20 degrees.

The low gravity on the Moon resulted in reduction of frictional forces between soil particles, observed as the increase in sinkage of wheel. Consequently, the effect of cohesion would become more significant in lunar gravity. An investigation into the relative influence of cohesion both at 1 G and at 1/6 G using DEM is recommended. Moreover, successive study on metrics for all wheel candidates in lunar gravity by DEM is suggested to verify the effect of gravity on wheel parameters decided in this analysis.

Acknowledgements

This research was in part funded by NASDA, currently JAXA, as the cooperative research project for 2000–2003. The cooperation of the Chofu Aerospace Center (CAC), JAXA, is fully acknowledged for allowing the use of the sloped test bed for the experiment.

References

[1] JAXA. JAXA Vision–JAXA 2025–. http://www.jaxa.jp/about/2025/index_e.html, accessed on March 8, 2008.

[2] Nishida S, Wakabayashi S. A study on mobility platform of lunar work rover. In: Preprints 26th Int. Symposium on Space Technology and Science, Hamamatsu, 2008: 2008-k-57. (CD-ROM)

[3] Fujii H. DEM analysis for a wheel of lunar rover and regolith system interaction. Unpublished Bachelor of Agric. Sci. Thesis, Faculty of Agriculture, Kyoto University, Kyoto, 2001. (in Japanese)

[4] Freitag DR, Green AJ, Melzer KJ, Costes NC. Wheels for lunar vehicles. Journal of Terramechanics 1972; 8(3): 89–105.

[5] Green AJ, Melzer KJ. Performance of the Boeing LRV wheels in a lunar soil stimulant—Report 1 Effect of wheel design and soil. Technical Report M-71-10, Mobility and Environmental Division, U. S. Army Engineer Waterways Experiment Station, Vicksburg, Mississippi, 1971.

[6] Melzer, KJ. Performance of the Boeing LRV wheels in a lunar soil stimulant—Report 2 Effects of speed, wheel load, and soil. Technical Report M-71-10, Mobility

673 and Environmental Division, U. S. Army Engineer Waterways Experiment Station,
674 Vicksburg, Mississippi, 1971.

675 [7] Asnani V, Delap D, Creager C. The development of wheels for the Lunar Roving
676 Vehicle. Journal of Terramechanics 2009; 46: 89–103.

677 [8] Wong JY, Asnani VM. Study of the correlation between the performances of lunar
678 vehicle wheels predicted by the Nepean wheeled vehicle performance model and test
679 data. Proc. IMechE, Part D: Journal of Automobile Engineering 2008; 222: 1939–1954.

680 [9] Richter L, Hamacher H. Investigation the locomotion performance of planetary
681 microrovers with small wheel diameters and small wheel loads. In: Proc. 13th Int. Conf.
682 ISTVS, Munich, 1999: 719–726.

683 [10] Richter L, Ellery A, Gao Y, Michaud S, Schmitz N, Weiss S. A predictive wheel-soil
684 interaction model for planetary rovers validated in testbeds and against MER Mars rover
685 performance data. In: Proc. 10th European Conf. ISTVS, Budapest, 2006: 1–27.

686 [11] Iizuka K, Sato Y, Kuroda Y, Kubota T. Study on traversability with consideration of
687 wheeled forms for lunar and planetary exploration rovers. Trans. JSME 2006; 72(724):
688 148–153. (in Japanese)

689 [12] Wakabayashi S, Kohno Y, Nishida S. Evaluation of low-pressure mobility system for
690 lunar vehicle. In: Preprints 26th Int. Symposium on Space Technology and Science,
691 Hamamatsu, 2008: 2008-k-56. (CD-ROM)

692 [13] Cundall PA, Strack ODL. Discrete numerical model for granular assemblies.
693 Géotechnique 1979; 29(1): 47–65.

694 [14] Johnson KL. Contact mechanics. Cambridge University Press, Cambridge, 1985.

695 [15] Mindlin RD, Deresiewicz H. Elastic spheres in contact under varying oblique forces.
696 Journal of Applied Mechanics 1953; 20: 327–344.

697 [16] Sakaguchi E, Kawakami S, Tamura S, Tobita F. Simulation on discharging phenomena
698 of grains by distinct element method–Influence of shapes of element on flowing states.
699 Journal of The Japanese Society of Agricultural Machinery 1996; 58(4): 9–17. (in
700 Japanese)

701 [17] Feng YT, Owen DRJ. An energy based corner to contact algorithm. Discrete Element
702 Methods (Edited by Cook BK, Jensen RP), ASCE, 32–37, 2002.

703 [18] Asaf Z, Shmulevich I, Rubinstein D. Predicting soil-rigid wheel performance using
704 distinct element methods. Transactions of the ASABE 2006: 49(3); 607–616.

705 [19] Horner DA, Peters JF, Carrillo A. Large scale discrete element modelling of vehicle-
706 soil interaction. Journal of Engineering Mechanics 2001; 127(10): 10271032.

707 [20] Nakashima H, Konishi T, Toki Y. Numerical Analysis for Cone Penetration of
708 Mesoscopic Soil Model. In: Proc. of the Joint North America, Asia-Pacific ISTVS
709 Conference and Annual Meeting of Japanese Society for Terramechanics, Fairbanks,
710 June 23–26, 2007: 2007-31-0319, 1–9. (CD-ROM)

[21] Oida A, Ohkubo S, Schwanghart H. Effect of tire lug cross section on tire performance simulated by distinct element method. In: Proc. 13th Int. Conf. ISTVS, Munich, 1999: 345–352.

[22] Oida A, Ohkubo S. Application of DEM to simulate interaction between soil and tire lug. Agricultural & Biosystems Engineering 2000; 1(1): 1–6.

[23] Fujii H. An analysis of lugged wheel performance by DEM for the development of wheel for a lunar rover. Unpublished Master of Agric. Sci. Thesis, Division of Environmental Science & Technology, Graduate School of Agriculture, Kyoto University, Kyoto, 2003. (in Japanese)

[24] Nakashima H, Fujii H, Oida A, Momozu M, Kawase Y, Kanamori H, Aoki S, Yokoyama T. Parametric analysis of lugged wheel performance for a lunar microrover by means of DEM. Journal of Terramechanics 2007; 44(2): 153–162.

[25] Li JQ, Zou M, Jia Y, Ma WZ, Ren LQ, Li YW. Research the interaction between the rigid wheel and the lunar soil by DEM. In: Proc. of the Joint North America, Asia-Pacific ISTVS Conference and Annual Meeting of Japanese Society for Terramechanics, Fairbanks, June 23–26, 2007: 1–12. (CD-ROM)

[26] Hopkins MA, Johnson JB, Sullivan R. Discrete element modeling of a rover wheel in granular material under the influence of Earth, Mars, and Lunar Gravity. In: Proc. Earth & Space 2008, 11th ASCE Aerospace Division International Conference on Engineering, Science, Construction, and Operations in Challenging Environments, Long Beach, March 3–5, 2008: 1–7. (CD-ROM)

[27] Nakashima H, Shioji Y, Kobayashi T, Aoki S. Numerical analysis of sand flow under low gravity condition. In: Proc. of the Joint North America, Asia-Pacific ISTVS Conference and Annual Meeting of Japanese Society for Terramechanics, Fairbanks, June 23–26, 2007: ISTVS-2007-62-0147, 1-10. (CD-ROM)

[28] Ji S, Shen HH. Contrasting terrestrial and lunar gravity: angle of repose and incline flows, In: Proceedings of 10th ASCE Aerospace Division International Conference on Engineering, Construction, and Operations in Challenging Environments, 2006: 1–8. (CD-ROM)

[29] Wakabayashi S, Matsumoto K. Development of slope mobility testbed using lunar soil. JAXA Research and Development Memorandum, JAXA-RM-05-003, 2006: 1–11. (in Japanese)

[30] Heiken GH, Vaniman DT, French BM, Ed. Lunar sourcebook. Cambridge University Press, Cambridge, 1991.

[31] Willman BM, Boles WW, McKay DS, Allen CC. Properties of lunar soil simulant JSC-1. Journal of Aerospace Engineering, ASCE, 1995; 8(2): 77–87.

[32] Momozu M, Oida A, Yamazaki M, Koolen AJ. Simulation of a soil loosening process by means of the modified distinct element method. Journal of Terramechanics 2003; 39: 207–220.

[33] Bui HH, Kobayashi T, Fukagawa R, Wells JC. Numerical and experimental studies of gravity effect on the mechanism of lunar excavations. Journal of Terramechanics 2009; 46: 115–124.